Astron. Astrophys. 187, 267–275 (1987)

ASTRONOMY AND ASTROPHYSICS

The cause of two plasma-tail disconnection events in comet P/Halley during the ICE-Halley radial period

J.W. Brosius [1,2], G.D. Holman [2], M.B. Niedner [2], J.C. Brandt [2,*], J.A. Slavin [3,], E.J. Smith [3], R.D. Zwickl [4], and S.J. Bame [4]**

[1] ST Systems Corporation, Lanham, MD 20706, USA
[2] Code 682, Laboratory for Astronomy and Solar Physics, NASA/Goddard Space Flight Center, Greenbelt, MD 20771, USA
[3] 169-506, Jet Propulsion Laboratory, 4800 Oak Grove Drive, Pasadena, CA 91109, USA
[4] Space Physics Group, Los Alamos National Laboratory, Los Alamos, NM 87545, USA

Received January 19, accepted March 19, 1987

Summary. We have examined ICE magnetometer and electron plasma data for possible causes of the plasma tail disconnection events (DE's) which were observed in Halley's comet on 1986 March 20–22 and April 11–12. We attribute the DE of March 20–22 to an interplanetary magnetic field polarity reversal, and the DE of April 11–12 to either a compression region in the solar wind, an interplanetary magnetic field polarity reversal, or a combination of the two. The measured average speeds of tail recession determined from pairs of successive photographs for both events vary between about 40 and 90 km s^{-1}, and the average acceleration determined from successive pairs of average velocity measurements is quite variable. The calculated times of disconnection for the two events are, in UT decimal dates, March 19.55 $\pm$ 0.16 and April 10.91 $\pm$ 0.36. Assuming that the two disconnection events are due to frontside reconnection after an interplanetary magnetic field reversal (the most likely explanation for the March 20–22 event, and one possible explanation for the April 11–12 event), we estimate that the time period between the onset of reconnection and the final disconnection of the tail is $0.1 \leqq \tau_{rec} \leqq 0.6$ day. This suggests that the average speed at which reconnection proceeds through the cometary magnetic field pile-up region is $1 \leqq v_{rec} \leqq 6$ km s^{-1}, or several tenths the local Alfvén speed.

Key words: comets – interplanetary medium

1. Introduction

For nearly a century, cometary plasma tails have been known to exhibit a variety of phenomena, including disconnection events, helical structures, ray folding, side rays, and kinks. Easily the most impressive of these is the disconnection event, in which the plasma tail is uprooted from the head and recedes from the head approximately along the sun-comet line. For an observational review of these structures and their probable solar wind causes, the reader is referred to Brandt and Mendis (1979), Ershkovich (1980), Brandt (1982), Jockers (1985), and Niedner (1986).

The solar wind was postulated based on observations of the gross behavior of cometary tails (Biermann, 1951), and the very existence of the tails themselves was suggested to depend upon the solar wind plasma dragging "frozen in" solar magnetic fields into the interplanetary medium and getting "hung up" in the cometary ionosphere (Alfvén, 1957). Wind-sock theory was used to infer the solar wind speed (and changes therein) as manifested by cometary plasma tail dynamical aberration angles (Brandt, 1961, 1967; Brandt and Rothe, 1976; Mendis and Ip, 1977), but not until the era of interplanetary spacecraft were these velocity changes, as well as changes in other parameters of the interplanetary medium (e.g., density, temperature, magnetic field strength and polarity) fully appreciated. Indeed, not until the encounter of the International Cometary Explorer (ICE) with comet Giacobini-Zinner on 1985 September 11 was Alfvén's (1957) draped magnetotail theory confirmed (Smith et al., 1986; Slavin et al., 1986a, b). We will refer to the dynamic parameters of the interplanetary medium (velocity and density) by the term "solar wind", and to the magnetic field parameters of the interplanetary medium (field strength and polarity) by the term "IMF" (interplanetary magnetic field). It is to the observed changes in the solar wind/IMF that numerous authors ascribe the observed cometary plasma tail phenomena (Niedner et al., 1978; Ip and Mendis, 1978; Niedner and Brandt, 1978, 1979; Ip, 1980; Ershkovich, 1980; Niedner, 1980, 1982, 1986; Ip and Axford, 1982; Saito et al., 1986; Russell et al., 1986).

In this paper we treat two disconnection events which occurred during the ICE – Halley radial period, 1986 March–April. As the photographic data-base of the International Halley Watch (IHW) network increases, additional phenomena will also be trated in some detail.

Several theories have been put forth to explain the occurrence of disconnection events. Among them are (i) the brute force dynamic pressure theory of Ip (1980), in which an enhancement in solar wind dynamic pressure simply compresses the cometary ionosphere out of existence, thus freeing the captured field lines which presumably confine the tail plasma to the head (Alfvén, 1957), allowing the tail to escape; (ii) the flute instability theory of

Send offprint requests to: J.W. Brosius [2]

* Present address: Laboratory for Atmospheric and Space Physics, Box 392, University of Colorado at Boulder, Boulder, CO 80309, USA
** Present address: Code 696, Laboratory for Extraterrestrial Physics, NASA/Goddard Space Flight Center, Greenbelt, MD 20771, USA

Ip and Mendis (1978), in which an enhancement in solar wind dynamic pressure lowers the growth time of the flute instability (to which the cometary ionosphere is marginally stable under quiescent conditions), temporarily enhancing the ionization of neutrals and ultimately depleting the ionosphere at a later time; (iii) the backside (near-tail) reconnection theory of Ip (1985) and Russell et al. (1986), in which either interplanetary shocks or variations in the Alfvén Mach number trigger reconnection on the tail side of the nucleus, in analogy to reconnection in the earth's magnetotail; and (iv) the frontside reconnection theory of Niedner and Brandt (1978, 1979), in which field lines of one predominant polarity are compressed against field lines of opposite polarity after an interplanetary sector boundary crossing, forcing the field lines which are draped around the comet head to undergo reconnection, severing the field lines from the comet head at the point of reconnection. The first three theories require enhanced solar wind ram pressure (in the compression region of a "high speed" stream, for example) in order to operate, while the latter theory requires a reversal of the IMF polarity (e.g., traversal of an interplanetary sector boundary). Russell et al. (1986), using the analogy of reconnection in the earth's magnetotail, also suggest that backside reconnection may be triggered by sudden changes in the direction of the IMF.

Ultimately, the question becomes the following: Do disconnection events correlate more closely with "streams" or with magnetic field polarity reversals (sector boundary crossings)? What makes the question so vexing is that sector boundaries frequently closely precede the compression regions (high density, low speed) of streams by $\leqq 1$ day, which in turn precede the high speed (low density) regions by $\leqq 1$ day, leaving some uncertainty concerning what actually does the work in bringing about a DE. There is not a one-to-one correspondence between sectors and streams (Niedner and Brandt, 1979), however, a fact which may be helpful in distinguishing which of the possible mechanisms actually cause DE's. In this paper, we make use of the photographs currently available through the IHW network, as well as in situ solar wind/IMF monitoring with the ICE spacecraft, in order to determine the mechanism responsible for two plasma tail disconnection events during 1986 March–April.

2. The data

Through the IHW Large-Scale Phenomena network, we currently have five good-quality photographs available for DE's of both 1986 March 20–22 and April 11–12 (see Figs. 1 and 2). The UT times and sources of these imagery are given in Table 1, and the relevant geometric parameters are given in Table 2.

Measurements of important quantities in the interplanetary medium – flow speed, density, magnetic field strength, and magnetic field polarity – were obtained with the ICE spacecraft. These are the primary data used to correlate solar wind/IMF features with DE's. These data are, to some extent, supplemented by Vega-1 magnetometer data (Schwingenschuh, 1986) and interplanetary solar neutral sheet maps (Hoeksema, 1986).

We seek to correlate the DE's of March 20 and April 11 with "high-speed" streams and/or IMF polarity reversals (sector boundary crossings). A sector boundary is defined as the boundary between a region in which the field lines are directed primarily toward the sun (in the ecliptic plane) and a region in which the field lines are directed primarily away from the sun (in the ecliptic plane). The angle of the field projected onto the ecliptic plane, or longitude angle φ_{xy}, is the traditional probe of such crossings. To first order any frontside reconnection process should not be sensitive to the sun-comet x-component of the field, however, and in this paper we use the two-dimensional "clock angle" φ_{yz} ($\phi_{yz} = \arctan(B_z/B_y)$) which includes the component of the magnetic field perpendicular to the ecliptic plane (z), and the component perpendicular to the sun-comet line in the plane of the ecliptic (y). A polarity reversal is encountered when the clock angle undergoes a 180° change, and such changes usually correspond to the traditional sector boundary crossing, in which ϕ_{xy} changes by $\sim 180°$. We look for correlations between DE's and 180° changes in ϕ_{yz}. Typically, the dynamic pressure of the solar wind is greatest in the compression region of a stream, where the density is elevated above average values; it is to such compression regions that we also look for correlations with disconnection events.

3. Data reduction and analysis

3.1. Derivation of times of disconnection

Because in most instances we lacked the original glass plates or good contact film copies of the originals, the measurements described below were made on enlargement photographic prints. For each photograph, a pair of SAO reference stars was selected, and the position of the detached end of the tail was measured with respect to the reference line connecting the stars by means of a finely-scaled ruler and a protractor. These measurements and the measured length of the reference line were entered into a computer program which calculates the coordinates (RA and Dec) of the severed tail, the coordinates of the nucleus at the time of observation, and the linear distance (km) of the detached tail from the nucleus on the assumption that the tail is oriented along the prolonged radius vector. The astrometry performed on the tail is considered accurate to $\leqq 20''$.

The average velocity v_{av} of the front edge of the disconnected tail during a given time interval is obtained by dividing the distance traveled by the change in mid-times of exposure between the corresponding photographs. Under the assumption of uniformly accelerated motion, the average velocity was taken to occur at the center of the time interval over which the average velocity was calculated. The average acceleration a_{av} was obtained by dividing the average velocity change by the corresponding time interval. In Table 3 we list results for the two disconnection events studied in this paper. The decimal date is given in Universal Time (UT), the distance of the front edge of the disconnected tail from the nucleus (x) is given in km, v_{av} is in km s^{-1}, and a_{av} is in cm s^{-2}.

From the equations of uniformly accelerated rectilinear motion, we obtain the time of disconnection t_D as

$$t_D = t_i - \left(\frac{v_i - v_0}{a}\right), \tag{1}$$

where v_i, the instantaneous speed inferred at time t_i under the assumption of uniform acceleration, is given by

$$v_i = v_{av(i,\,i+1)} - a\left(\frac{t_{i+1} - t_i}{2}\right), \tag{2}$$

and v_0, the "initial speed" when the tail first disconnects from the head, is given by

$$v_0 = (v_i^2 - 2ax_i)^{1/2}, \tag{3}$$

1987A&A...187..267B

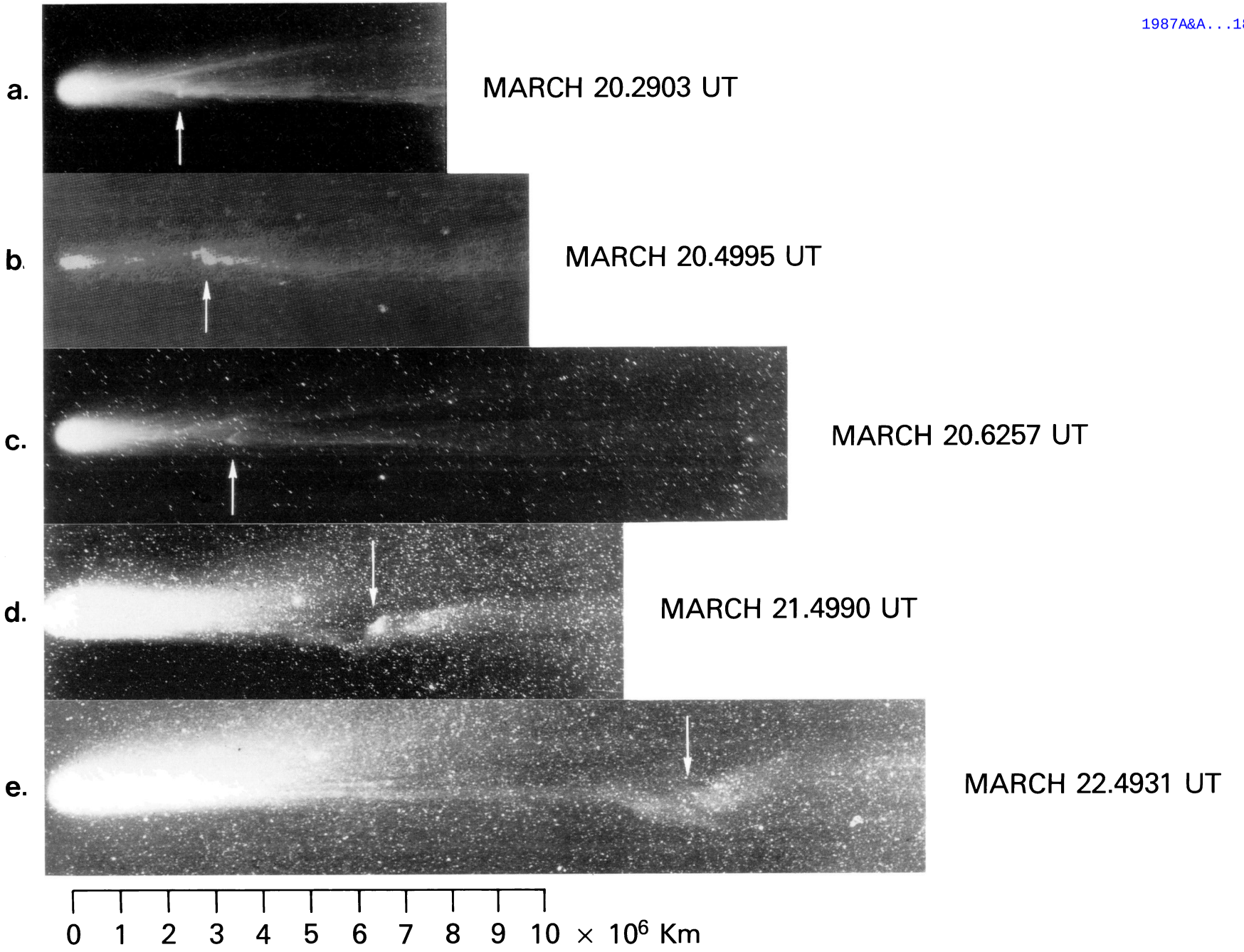

Fig. 1a–e. 1986 March 20–22 photographic sequence of Halley's comet showing the development of the first disconnection event (DE) studied in this paper. The images were obtained: **a** March 20.2903 UT at Cerro Tololo Interamerican Observatory (University of Michigan Curtis Schmidt), **b** March 20.4995 UT at Table Mountain Observatory (University College London detector), **c** March 20.6257 UT at Mauna Kea Observatory, **d** March 21.4990 UT at Easter Island (part of International Halley Watch's "Island Network"), and **e** March 22.4931 UT at the Joint Observatory for Cometary Research. For additional observational details concerning the images, see Table 1. The arrows locate the near end of the rejected tail, whose linear separations from the nucleus are listed in Table 3. All photographs are printed at the same angular scale; the linear scale at the bottom of the figure yields distances along the prolonged radius vector at the mid-time of the sequence

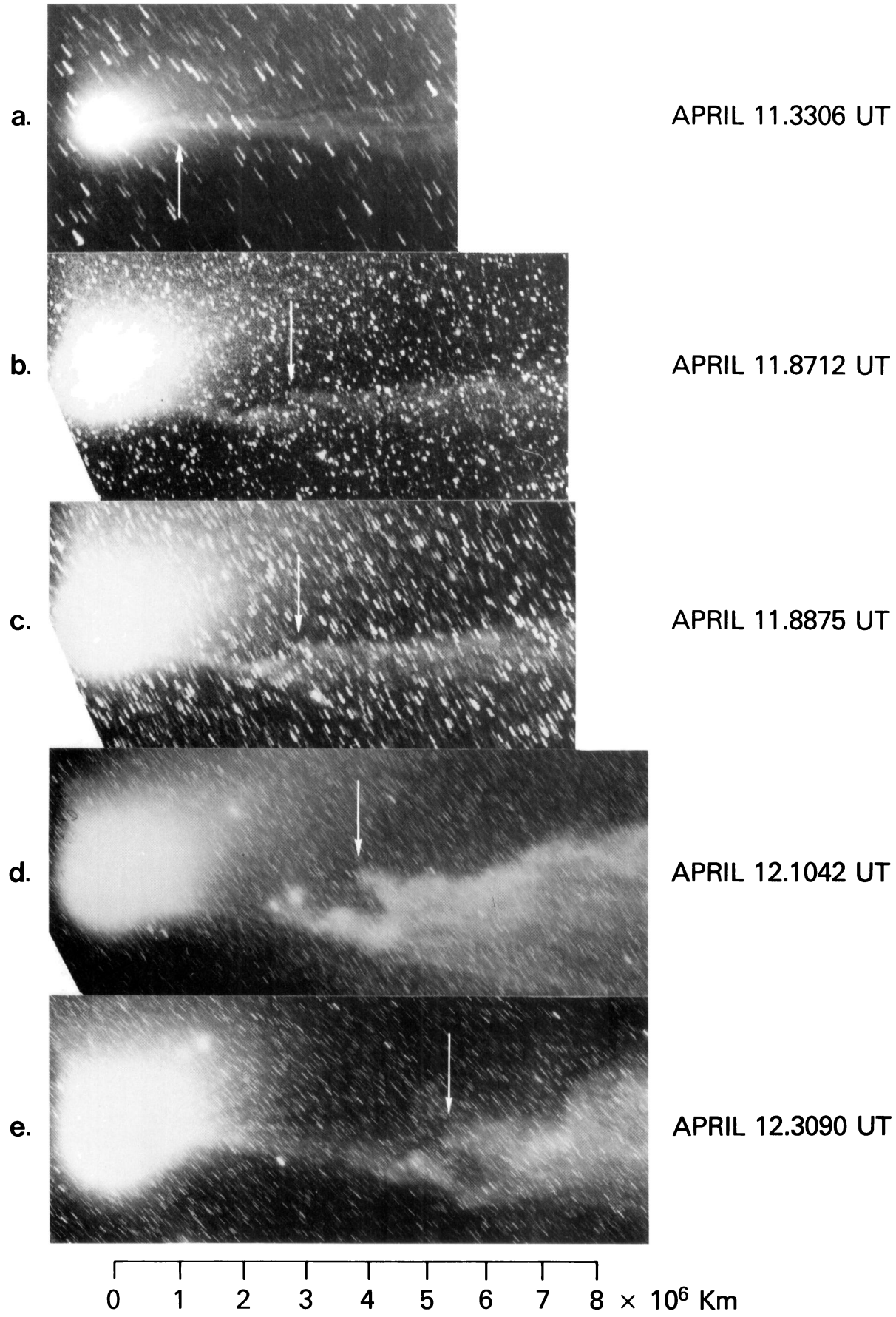

Table 1. Photographic observations used in the analysis of the disconnection events of march 20–22 and april 11–12

Obs. no. (this paper)	Mid-exposure (UT)	Source	Plate no.	Exp. length (min)	Emulsion	Filter
March 20–22 event						
1.	March 20.2903	Univ. Mich. Curtis Schmidt (CTIO)	29953	20	IIa-O	–
2.	March 20.4995	Univ. Col. London (Table Mtn Obs.)	–	20	Imaging photon det.	CO^+
3.	March 20.6257	Mauna Kea Observatory	–	30	IIIa-J	–
4.	March 21.4990	IHW "Island Net" – Easter Island	S-134	16	2415TP	–
5.	March 22.4931	Joint Obs. for Cometary Res. (JOCR)	S-2049	10	IIa-O	–
April 11–12 event						
1.	April 11.3306	IHW "Island Net" – Tahiti	–	30	2415TP	W47B
2.	April 11.8712	IHW "Island Net" – Reunion I.	–	9	2415TP	–
3.	April 11.8875	IHW "Island Net" – Reunion I.	–	20	2415TP	–
4.	April 12.1042	Univ. Mich. Curtis Schmidt (CTIO)	30065	20	103a-O	–
5.	April 12.3090	Univ. Mich. Curtis Schmidt (CTIO)	30072	20	103a-O	–

Table 2. Geometric parameters used in the analysis of the disconnection events of march 20–22 and april 11–12

Obs. no.	Mid-exposure	Δ [a]	β [b]	R_H [c]	R_I [d]	θ_{HE} [e]	θ_{IH} [f]
March 20–22 event							
1.	March 20.2903	0.8032	113.9	0.9972	0.9303	47.93	−15.59
2.	March 20.4995	0.7979	113.9	1.0004	0.9304	47.51	−15.14
3.	March 20.6257	0.7948	113.9	1.0023	0.9305	47.26	−14.87
4.	March 21.4990	0.7727	113.9	1.0157	0.9308	45.55	−13.05
5.	March 22.4931	0.7477	114.1	1.0309	0.9312	43.63	−11.00
April 11–12 event							
1.	April 11.3306	0.4174	149.1	1.3371	0.9426	9.56	25.51
2.	April 11.8712	0.4184	150.6	1.3454	0.9430	8.72	26.42
3.	April 11.8875	0.4185	150.6	1.3456	0.9430	8.70	26.44
4.	April 12.1042	0.4191	151.2	1.3489	0.9432	8.36	26.80
5.	April 12.3090	0.4198	151.7	1.3521	0.9433	8.04	27.14

[a] Δ = geocentric distance of Halley in AU
[b] β = tail foreshortening angle in degrees
[c] R_H = heliocentric distance of Halley in AU
[d] R_I = heliocentric distance of ICE in AU
[e] θ_{HE} = Halley-Earth longitude difference in degrees (positive indicates Halley leads)
[f] θ_{IH} = ICE-Halley longitude difference in degrees (positive indicates ICE leads)

and where $i = 1, 2, 3, 4, 5$ correspond to the five observations of x, t for each of the two events. The velocities and accelerations in Tables 3 and 4 are well within the range of values quoted by previous authors (Mendis and Ip, 1977; Niedner, 1981; Guerin et al., 1986). The observed variability in acceleration may be a manifestation of the expectation that different forces (e.g., Lorentz force and solar wind dynamic pressure force) dominate the disconnected tail motions at different distances from the nucleus, as well as the expectation that these individual forces vary with position and/or time. Some combinations of data points yield an imaginary initial speed, probably due to the non-uniform acceleration. These imaginary values are listed along with the real values in Table 4.

Combining the results for the various trios of x, t listed in Table 4 for each of the two disconnection events, we obtain t_D = March 19.55 ± 0.16 for the event of March 20, and t_D = April

Fig. 2a–e. 1986 April 11–12 photographic sequence showing the development of the second DE studied. The images were obtained **a** April 11.3306 UT at Tahiti (part of the IHW's "Island Network"), **b** April 11.8712 UT and **c** April 11.8875 UT at Reunion Island (part of the IHW's "Island Network"), **d** April 12.1042 UT and **e** April 12.3090 UT at CTIO/University of Michigan Curtis Schmidt. For additional details concerning the photographs, refer to Table 1. The arrows locate the near end of the rejected tail, whose linear separations from the nucleus are listed in Table 3. All photographs are printed at the same angular scale; the linear scale at the bottom of the figure yields distances along the prolonged radius vector at the mid-time of the sequence

Table 3. Distance, average velocity, and average acceleration of the front edge of the disconnected tail for the disconnection events of March 20 and April 11

Obs. no.	t = date (UT)	x (km)	v_{av} (km s^{-1})	a_{av} (cm s^{-2})
1	3/20.2903	2.43 10^6		
			40.4	
2	3/20.4995	3.16 10^6		− 23.0
			37.0	
3	3/20.6257	3.56 10^6		3.1
			38.4	
4	3/21.4990	6.46 10^6		50.9
			79.5	
5	3/22.4931	1.33 10^7		
1	4/11.3306	1.08 10^6		
			42.7	
2	4/11.8712	3.07 10^6		46.9
			54.0	
3	4/11.8875	3.15 10^6		− 18.8
			52.1	
4	4/12.1042	4.12 10^6		215.6
			91.3	
5	4/12.3090	5.74 10^6		

Table 4. The measured average acceleration, and the calculated initial speed and time of disconnection for various trios of data points for the disconnection events of March 20 and April 11. The symbol "j" denotes imaginary initial speeds

Obs. trio	a_{av} (cm s^{-2})	t_D (date)	v_0 (km s^{-1})
March 20–22 event			
1, 2, 3	− 23.0	19.71	54.0
2, 3, 4	3.1	19.47	34.1
3, 4, 5	50.9	–	57.1j
1, 2, 4	− 4.1	19.62	43.2
1, 3, 4	− 1.4	19.58	40.2
1, 2, 5	19.3	19.39	23.6
April 11–12 event			
1, 2, 3	46.9	10.55	2.1j (~0)
2, 3, 4	− 18.8	11.27	63.9
3, 4, 5	215.6	–	112.1j
1, 2, 4	28.5	10.93	26.2
1, 3, 4	27.1	10.94	27.3
1, 2, 5	65.8	–	26.0j

10.91 ± 0.36 for the event of April 11 (all dates are given as UT decimal dates). These ranges in disconnection time reflect the observed variability in acceleration, and the corresponding error associated with the assumption of uniform acceleration. A better knowledge of disconnected plasma tail motions for distances less than 10^6 km from the nucleus are needed in order to reduce the uncertainties. Recently, Jockers et al. (1986) have obtained a sequence of photographs of the event of April 11 when the front edge of the disconnected tail was less than 10^6 km from the nucleus; our disconnection time of April 10.91 agrees with their observations. Concerning the March event, a visible/UV outburst in comet Halley, beginning March 18.8, has been reported by Feldman et al. (1986). Such outbursts may be attributed to sector boundary crossings and the ensuing reconnection process (Niedner, 1980). It is therefore possible that the outburst reported by Feldman et al. (1986) marks the arrival of an IMF polarity reversal and the onset of reconnection. We will pursue this further in the Discussion section.

3.2. *The solar wind and IMF measured by ICE*

The corotation time from Halley to ICE is given, to first order, by

$$\Delta t = \frac{\theta_2 - \theta_1}{\Omega} + \frac{R_2 - R_1}{V_{sw}}, \tag{4}$$

where $\theta_2 - \theta_1$ is the angular separation between ICE and Halley in the plane of the solar equator (where angles are taken to increase in the direction of solar rotation), Ω is the sideral equatorial angular rotation velocity of the sun ($14.^\circ4\,\text{day}^{-1}$), R_2 and R_1 are the heliocentric distances of ICE and Halley, and V_{sw} is the solar wind speed. High-order corrections take into account ICE's motion during the first order corotation interval and are incorporated by an iterative procedure in a computer code. The average solar wind speed at 1 AU is 400 km s^{-1}, but since we do not know a priori what the solar wind speed is at Halley at the time of the DE, we calculate a range in Δt based on the observation that the solar wind speed typically ranges between 300 and 700 km s^{-1}. The geometrical parameters used in the corotation procedure are listed in Table 2.

For the DE of March 20, we obtain corotation times of −1.63 days, −1.54 days, and −1.43 days for solar wind speeds of 300, 400, and 700 km s^{-1}, respectively; for the event of April 11, we obtain corotation times of −0.58 day, 0.04 day, and 0.82 days for the same solar wind speeds. A negative sign means that the feature arrived at ICE before it arrived at Halley. Combining these with the times of disconnection obtained earlier, we obtain the times of disconnection mapped to ICE, which to first order indicates at what times the responsible solar wind feature(s) would have swept by the spacecraft. The corotation time for the March 20 event is relatively insensitive to the solar wind speed because the radial separation between ICE and Halley is small (~0.04 AU). The corotation time for the April 11 event has a fairly strong dependence on solar wind speed due to a significant radial separation (~0.37 AU); however, an examination of ICE electron plasma data during the time interval obtained by combining the disconnection and corotation times shows that $300\,\text{km s}^{-1} < V_{sw} < 400\,\text{km s}^{-1}$ (see Fig. 4), suggesting that the more appropriate corotation time range is −0.58 day to 0.04 day. The "disconnection windows" at ICE for the two events are therefore

$$t_{ICE}\,(\text{March 20}) = 18.02 \pm 0.26,$$

and

$$t_{ICE}\,(\text{April 11}) = 10.64 \pm 0.67.$$

These windows are marked as solid lines on the ICE electron plasma and magnetometer data shown in Figs. 3 and 4. We now consider additional possible sources of uncertainty before examining the ICE data during these time intervals.

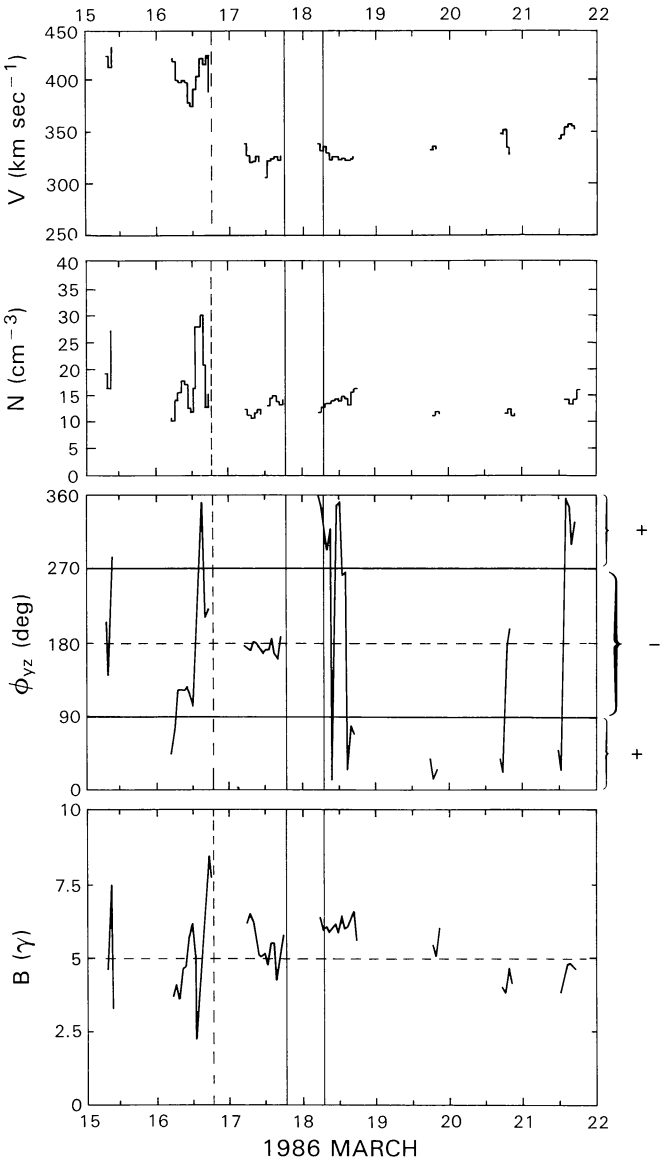

Fig. 3. The solar wind flow speed (a) in km s^{-1} and the solar wind electron number density (b) in cm^{-3} from the ICE electron plasma experiment around the time of the March 20 DE. The interplanetary magnetic field clock angle ϕ_{yz} (c) and the magnetic field strength (d) in units of 10^{-5} Gauss ($=1\gamma$) from the ICE magnetometer around the time of the March 20 DE. The solid lines indicate the arrival window as calculated in the text, and the dashed line allows for an additional 1 day response time. The IMF is directed predominantly toward the sun for $90° \leqq \phi_{yz} \leqq 270°$

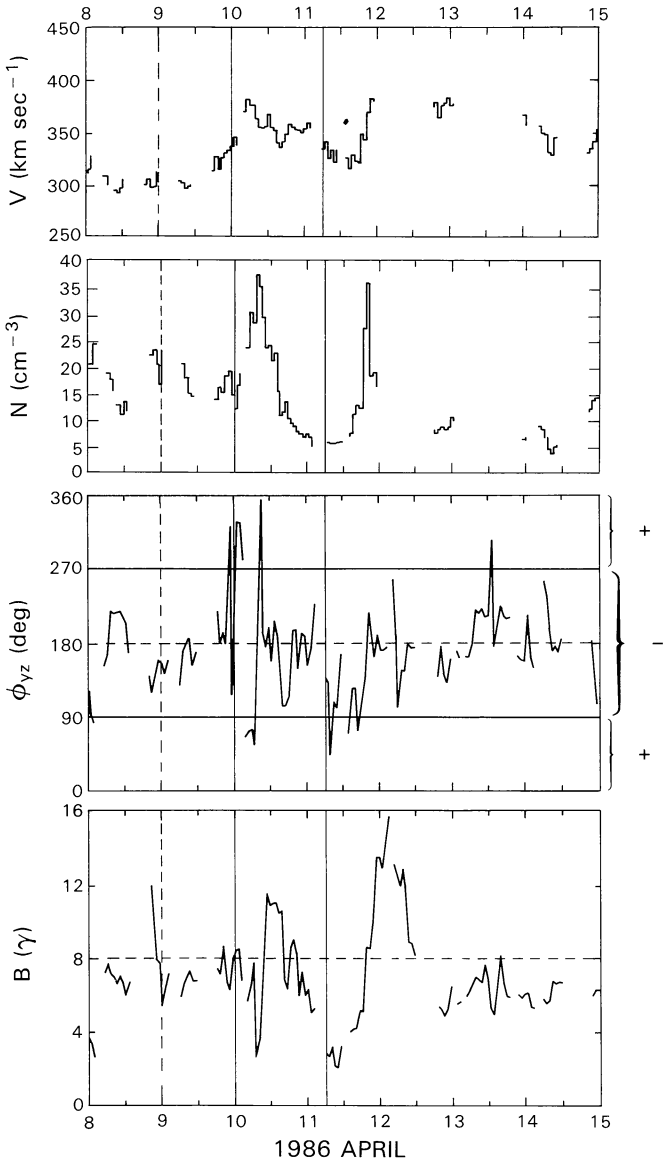

Fig. 4. The solar wind flow speed (a) in km s^{-1} and the solar wind electron number density (b) in cm^{-3} from the ICE electron plasma experiment around the time of the April 11 DE. The interplanetary magnetic field clock angle ϕ_{yz} (c) and the magnetic field strength (d) in units of 10^{-5} Gauss ($=1\gamma$) from the ICE magnetometer around the time of the April 11 DE. The solid lines indicate the arrival window as calculated in the text, and the dashed line allows for an additional 1 day response time

The response time between the arrival of a solar wind feature and the onset of an observable cometary phenomenon is not a well known parameter. Niedner (1980, 1982) and Niedner and Brandt (1978) estimate a time period $\tau_{rec} \sim 0.5$–1.0 day from the onset of frontside reconnection to a final disconnected tail. Ip and Mendis (1978) estimate the growth time for the flute instability to be $\tau_f \sim 1$ h, based on pre-Halley Encounter estimates of the relevant parameters. We compensate for the uncertain response time for any agent causing a disconnection event by expanding the front edge of the ICE arrival windows listed above by 1.0 day, obtaining March 16.76–18.28 and April 8.97–11.31. It is these windows which we examine (see Figs. 3 and 4) for solar wind features responsible for the observed disconnection events. The inclusion of a response time in the ICE arrival window does not affect the arguments concerning the observed solar wind speed in the arrival window which were used to narrow the arrival window for the April 11 event (i.e., no solar wind speeds outside the range $300 < V_{sw} < 400$ km s^{-1} were found between April 8.97 and 9.97).

An additional possible source of uncertainty which we mention, but at present do not incorporate in a detailed way, is the heliographic latitude difference between ICE and Halley for the March 20 ($-1\overset{\circ}{.}6$) and April 11 ($-11\overset{\circ}{.}5$) events. It is possible that the solar wind and IMF properties at ICE are different from those at Halley, especially for the April 11 event. For example, Rhodes

and Smith (1975, 1976) found a dependence of solar wind speed on heliographic latitude $\sim 13\,\mathrm{km\,s^{-1}\,deg^{-1}}$, while Schwenn et al. (1978) found that a high speed stream which was observed at one satellite was not observed at another, separated by only 10° in latitude from the first. There is no way to be certain that the solar wind speed, density, field strength, or polarity measured near the ecliptic plane (with ICE) are representative of those same quantities at Halley. Independent analysis of the orientation and latitude extent of the solar neutral sheet presumed to be responsible for the interplanetary sector structure (Rosenberg and Coleman, 1969; Smith et al., 1978) may be done by extrapolating the observed solar photospheric magnetic field out to a "source surface" via multipole expansion (Svalgaard and Wilcox, 1978). The extension of the resulting coronal neutral line into the interplanetary medium beyond the source surface is assumed to be radial. Such calculations have been provided by Hoeksema (1986), and the resulting neutral sheet maps agree reasonably well with spacecraft measurements in that the extrapolated sector crossings in the ecliptic plane usually occur where ICE and Pioneer Venus Orbiter (PVO) spacecraft measure them to occur (Niedner, 1986). There is, however, sometimes substantial disagreement (of several days) between the location of the crossing as determined by spacecraft and the location of the crossing as determined by neutral sheet maps (Niedner, 1986). We therefore feel that using the neutral sheet maps to incorporate further corrections to the corotation times between ICE and Halley due to neutral sheet tilt angles and ICE/Halley latitude differences would not be justified. Nevertheless, for the sake of completeness, we note that the neutral sheet tilt angles derived from the coronal neutral line maps yield corrections of +0.15 day for the March 20 DE and −0.61 day for the April 11 DE. These corrections do not change the arguments in what follows.

The disconnection windows at ICE are shown as solid lines in Figs. 3 and 4; the dashed lines indicate the early edges of the arrival windows at ICE if a response time of 1 day is assumed. We give below the salient features of the solar wind/IMF in the arrival windows, and discuss their possible relation to the observed DE's.

For the March 20 event, the arrival window extends from March 16.76 to 18.28. The flow speed remains between 300 and $430\,\mathrm{km\,s^{-1}}$ throughout the entire window. The magnetic field is of mixed polarity on the 16th; the predominant polarity prior to the 16th cannot be determined from the ICE data because there is essentially no data for the preceding ~4 days, but Vega-1 data currently available to the authors (Schwingenschuh, 1986) suggest a sector (of predominantly inward polarity) of ~2–3 days duration. A 12-h data gap extends from March 16.69 to March 17.19. After the gap, the field strength, polarity, and electron density remain fairly constant for 12 hours. After another 12-h data gap, the electron density and field strength maintain their pre-gap values, but the magnetic field polarity is rotated by 180°. Although the data on the following days are sparse, it appears that the new (predominantly outward) polarity persists for at least 6 days.

Clearly, there is one feature observed in the ICE arrival window for the March 20 DE to which the DE may be attributed: a magnetic field polarity reversal occurring during the data gap between March 17.67 and March 18.17. We conclude that this magnetic field polarity reversal which occurred well withinn the ICE arrival window, without assumption of response time, is the most likely cause of the event. Note, however, the compression region of several hours duration which occurred around the middle of the 16th (the density maintained a peak value of $\sim 30\,\mathrm{cm^{-3}}$ for ~1.7 h). It is possible that a similar short-lived compression region, with solar wind and IMF signatures hidden in the data gaps, may also be responsible for the DE. (The possibility that a short-lived compression region occurred in the same data gap within which the polarity reversal occurred will be settled after further acquisition of Vega-1 data).

For the April 11 event, the arrival window extends from April 8.97 to 11.31. The flow speed remains between 300 and $400\,\mathrm{km\,s^{-1}}$ throughout the entire window. The clock angle and field strength remain constant through most of the 9th. A magnetic field polarity reversal of ~0.5 day duration occurs between April 9.88 and April 10.42. Near the end of this polarity reversal the field strength and the electron plasma density undergo steep, short-term enhancements. The field strength and electron density then drop to their lowest values in about a 7-day interval, before increasing to their highest respective values in the same 7-day interval. The density remains at about $38\,\mathrm{cm^{-3}}$ between 1900 UT and 2100 UT on the 11th, outside of the arrival window. The field polarity is turbulent, but remains fairly steadily at 180° after the 0.5 day reversal on the 9th–10th.

There are two features in the ICE arrival window to which the DE of April 11 may be attributed: a polarity reversal, and a compression region which occurs essentially simultaneously with the polarity reversal. It is impossible to determine whether one or the other, or both in concert, brought about this DE. Indeed, with such a large heliographic latitude separation between ICE and Halley for this event (11°5), we cannot rule out the possibility that the compression region outside of the arrival window, or even some solar wind/IMF feature not measured by ICE, brought about this DE.

4. Discussion

Our primary conclusions are that the DE of March 20–22 was most likely caused by an IMF polarity reversal, and the DE of April 11–12 could have been caused by a compression region, an IMF polarity reversal, or a combination of the two. We discuss some implications of these conclusions in this section.

For the March 20 event, the earliest and latest possible times at which the IMF polarity reversal could have occurred at ICE are March 17.67 and 18.17; these times correspond to the beginning and the end of the data gap within which the polarity reversed (see Fig. 3). Using the corotation time of $+1.53 \pm 0.10$ days from ICE to Halley, the earliest and latest possible times at which the polarity reversal could have arrived at Halley are March 19.10 and 19.80. The latest possible disconnection time, March 19.71, is 0.61 day after the earliest possible arrival of the polarity reversal. Since the polarity reversal must have arrived at Halley before the onset of disconnection (assuming that frontside reconnection is the appropriate mechanism), we find that $0.0\ \mathrm{day} \leqq \tau_{rec} \leqq 0.61\ \mathrm{day}$. This is not inconsistent with the results of Niedner (1980, 1982) and Niedner and Brandt (1978), but places a tight restriction on the reconnection timescale. A similar calculation for the April 11 event, again assuming frontside reconnection, yields $0.09\ \mathrm{day} \leqq \tau_{rec} \leqq 1.43\ \mathrm{day}$. Since, however, the polarity reversal itself lasts only 0.54 day, and since the timescale required for reconnection to operate cannot exceed the lifetime of the IMF feature driving reconnection if a totally detached tail is to result, we obtain $0.09\ \mathrm{day} \leqq \tau_{rec} \leqq 0.54\ \mathrm{day}$. This result is consistent with that for the March 20 DE.

Assuming that the reconnection time scale τ_{rec} corresponds to the travel time of the reconnection diffusion region across the magnetic field pile-up region (Neubauer et al., 1986) between the "collisionopause" (Réme et al., 1986) and the contact surface

(Balsiger et al., 1986; Reinhard, 1986), we can calculate the average speed v_{rec} at which reconnection occurs in the pile-up region. With an average distance of 5.5 10^4 km between the collisionopause and the nucleus along the sun-comet line (Rème et al., 1986), and an average distance of 4.7 10^3 km between the contact surface and the nucleus along the sun-comet line (Balsiger et al., 1986; Reinhard, 1986), we obtain $1.0 \leqq v_{rec} \leqq 6.4\ km\ s^{-1}$ for the reconnection time scales quoted above. For the magnetic field strength of $30\gamma \leqq B \leqq 70\gamma$ (Neubauer et al., 1986; Riedler et al., 1986) and the electron number density of $100\ cm^{-3} \leqq n_e \leqq 4000\ cm^{-3}$ (Grard et al., 1986) measured in the pile-up region (where 4000 cm^{-3} was measured just before instrument failure), we estimate the Alfvén speed $\sim 5.7\ km\ s^{-1} \leqq V_A \leqq \sim 15\ km\ s^{-1}$. It is interesting that v_{rec} is comparable to the Petschek reconnection rate, ~ 0.1 to $1.0\ V_A$ (cf. Sonnerup, 1985).

Diffusion region properties (dimensions and resistivity) have been studied by Niedner et al. (1981) based on $\tau_{rec} \sim 0.75$ days along with estimates of other cometary parameters. With actual measurements (not estimates) of cometary parameters from the Halley and Giacobini-Zinner Encounters, along with the reconnection time scales obtained in this paper, an improved study of the reconnection process in cometary atmospheres can now be made. This topic will be pursued in a later paper.

It is interesting that the outburst of March 18.8 reported by Feldman et al. (1986) occurred so close in time to the commencement of a spectacular disconnection event. Either the visibility of the DE was enhanced by the outburst (loading CO_2^+ ions into the tail), or the outburst itself was a result of the solar wind/IMF feature (presumably IMF polarity reversal in this case) giving rise to the DE. As discussed earlier in this section, the earliest and latest possible arrivals of the IMF polarity reversal at Halley were March 19.10 and March 19.80. Thus the polarity reversal arrived 0.3–1.0 day after the onset of the outburst. It thus seems unlikely that the outburst may be attributed to frontside reconnection during an IMF polarity reversal.

Acknowledgements. This work was supported in part by the ISEE/ICE Guest Investigator Program. The research performed at the Jet Propulsion Laboratory of the California Institute of Technology was carried out under contract to the National Aeronautics and Space Administration. The work done at Los Alamos National Laboratory was under the auspices of the United States Department of Energy with support from NASA under S-04039-D.

References

Alfvén, H.: 1957, *Tellus* **9**, 92
Balsiger, H., Altwegg, K., Buhler, F., Geiss, J., Ghielmetti, A.G., Goldstein, B.E., Goldstein, R., Huntress, W.T., Ip, W.-H., Lazarus, A.J., Meier, A., Neugebauer, M., Rettenmund, U., Rosenbauer, H., Schwenn, R., Sharp, R.D., Shelley, E.G., Ungstrup, E., Young, D.T.: 1986, *Nature* **321**, 330
Biermann, L.: 1951, *Z. Astrophys* **29**, 274
Brandt, J.C.: 1961, *Astrophys. J.* **133**, 1091
Brandt, J.C.: 1967, *Astrophys. J.* **147**, 201
Brandt, J.C.: 1982, in *Comets*, ed. L.L. Wilkening, University of Arizona Press, p. 519
Brandt, J.C., Mendis, D.A.: 1979, in *Solar System Plasma Physics*, eds. C.F. Kennel, L.J. Lanzerotti, E.N. Parker, North-Holland, Amsterdam, p. 255
Brandt, J.C., Rothe, E.D.: 1976, in *The Study of Comets*, ed. B. Donn et al., NASA SP-393, p. 878
Ershkovich, A.I.: 1980, *Space Sci. Rev.* **25**, 3
Feldman, P.D., A'Hearn, M.F., Festou, M.C., McFadden, L.A., Weaver, H.A., Woods, T.N.: 1986, *Nature* **324**, 433
Grard, R., Pedersen, A., Trotignon, J.-G., Beghin, C., Mogilevsky, M., Mikhailov, Y., Molchanov, O., Formisano, V.: 1986, *Nature* **321**, 290
Guerin, P., Koutchmy, S., Vial, J.C.: 1986, *Astron. Astrophys.* **167**, 395
Hoeksema, T.: 1986 (private communication)
Ip, W.-H.: 1980, *Astrophys. J.* **238**, 388
Ip, W.-H.: 1985, ESA SP-235, Proc. ESA Workshop on *Future Missions in Solar, Heliospheric, and Space Plasma Physics*, p. 65
Ip, W.-H., Axford, W.I.: 1982, in *Comets*, ed. L.L. Wilkening, University of Arizona Press, Tucson, p. 588
Ip, W.-H., Mendis, D.A.: 1978, *Astrophys. J.* **223**, 671
Jockers, K.: 1985, *Astron. Astrophys. Suppl.* **62**, 791
Jockers, K., Geyer, E.H., Rosenbauer, H., Hanel, A.: 1986, 20th ESLAB Symp., ESA SP-250, Vol. **I**, p. 51
Mendis, D.A., Ip, W.-H.: 1977, *Space Sci. Rev.* **20**, 145
Neubauer, F.M., Glassmeier, K.H., Pohl, M., Raeder, J., Acuna, M.H., Burlaga, L.F., Ness, N.F., Musmann, G., Mariani, F., Wallis, M.K., Ungstrup, E., Schmidt, H.U.: 1986, *Nature* **321**, 352
Niedner, M.B.: 1980, *Astrophys. J.* **241**, 820
Niedner, M.B.: 1981, *Astrophys. J. Suppl.* **46**, 141
Niedner, M.B.: 1982, *Astrophys. J. Suppl.* **48**, 1
Niedner, M.B.: 1986, *Adv. Space Res.* **6**, 315
Niedner, M.B., Brandt, J.C.: 1978, *Astrophys. J.* **223**, 655
Niedner, M.B., Brandt, J.C.: 1979, *Astrophys. J.* **234**, 723
Niedner, M.B., Ionson, J.A., Brandt, J.C.: 1981, *Astrophys. J.* **245**, 1159
Niedner, M.B., Rothe, E.D., Brandt, J.C.: 1978, *Astrophys. J.* **221**, 1014
Reinhard, R.: 1986, *Nature* **321**, 313
Reme, H., Sauvaud, J.A., d'Uston, C., Cotin, F., Cros, A., Anderson, K.A., Carlson, C.W., Curtis, D.W., Lin, R.P., Mendis, D.A., Korth, A., Richter, A.K.: 1986, *Nature* **321**, 349
Rhodes, E.J., Smith, E.J.: 1975, *J. Geophys. Res.* **80**, 917
Rhodes, E.J., Smith, E.J.: 1976, *J. Geophys. Res.* **81**, 2123
Riedler, W., Schwingenschuh, K., Yeroshenko, Y.G., Styashkin, V.A., Russell, C.T.: 1986, *Nature* **321**, 288
Rosenberg, R.L., Coleman, P.J.: 1969, *J. Geophys. Res.* **74**, 5611
Russell, C.T., Saunders, M.A., Phillips, J.L., Fedder, J.A.: 1986, *J. Geophys. Res.* **91**, 1417
Saito, T., Yumoto, K., Hirao, K., Saito, K., Nakagawa, T., Smith, E.J.: 1986, *Geophys. Res. Letters* **13**, 821
Schwenn, R., Montgomery, M.D., Rosenbauer, H., Miggenrieder, H., Muhlhauser, K.H., Bame, S.J., Feldman, W.C., Hansen, R.T.: 1978, *J. Geophys. Res.* **83**, 1011
Schwingenschuh, K.: 1986 (private communication)
Slavin, J.A., Goldberg, B.A., Smith, E.J., McComas, D.J., Bame, S.J., Strauss, M.A., Spinrad, H.: 1986a, *Geophys. Res. Letters* **13**, 1085
Slavin, J.A., Smith, E.J., Tsurutani, B.T., Siscoe, G.L., Jones, D.E., Mendis, D.A.: 1986b, *Geophys. Res. Letters* **13**, 283
Smith, E.J., Tsurutani, B.T., Rosenberg, R.L.: 1978, *J. Geophys. Res.* **83**, 717
Smith, E.J., Tsurutani, B.T., Slavin, J.A., Jones, D.E., Siscoe, G.L., Mendis, D.A.: 1986, *Science* **232**, 382
Sonnerup, B.U.O.: 1985, in *Unstable Current Systems and Plasma Instabilities in Astrophysics*, eds. M.R. Kundu, G.D. Holman, Reidel, Dordrecht, p. 5
Svalgaard, L., Wilcox, J.M.: 1978, *Ann. Rev. Astron. Astrophys.* **16**, 429